

**Stress field
sensitivity analysis in
a sedimentary
sequence**

T. Hergert et al.

Stress field sensitivity analysis in a sedimentary sequence of the Alpine foreland, Northern Switzerland

T. Hergert^{1,*}, O. Heidbach², K. Reiter^{2,3}, S. B. Giger⁴, and P. Marschall⁴

¹Karlsruhe Institute of Technology, Institute of Applied Geosciences, Adenauerring 20b, 76131 Karlsruhe, Germany

²GFZ German Research Centre for Geosciences, Sect. 2.6 Seismic Hazard and Stress Field, Telegrafenberg, 14473 Potsdam, Germany

³University of Potsdam, Inst. of Earth and Environmental Science, Karl-Liebknecht-Straße 24–25, 14476 Potsdam-Golm, Germany

⁴NAGRA, National Cooperative for the Disposal of Radioactive Waste, 5430 Wettingen, Switzerland

*now at: TU Darmstadt, Institute of Applied Geosciences, Schnittspahnstr. 9, 64287 Darmstadt, Germany

Received: 3 February 2015 – Accepted: 3 February 2015 – Published: 19 February 2015

Correspondence to: T. Hergert (hergert@geo.tu-darmstadt.de)

Published by Copernicus Publications on behalf of the European Geosciences Union.

Title Page

Abstract

Introduction

Conclusions

References

Tables

Figures

⏪

⏩

◀

▶

Back

Close

Full Screen / Esc

Printer-friendly Version

Interactive Discussion



Abstract

The stress field at depth is a relevant parameter for the design of subsurface constructions and reservoir management. Yet the distortion of the regional stress field due to local-scale features such as sedimentary and tectonic structures or topography is often poorly constrained. We conduct a stress sensitivity analysis using 3-D numerical geomechanical modelling with an elasto-plastic material law to explore the impact of such site specific features on the stress field in a sedimentary sequence of the Swiss Alpine foreland. The model's dimensions are 14 km × 14 km × 3 km and it contains ten units with different mechanical properties, intersected by two regional fault zones. An initial stress state is established involving a semi-empirical relationship between the ratio of horizontal to vertical stress and the overconsolidation ratio of argillaceous sediments. The model results indicate that local topography can affect the stress field significantly to depths greater than the relief contrasts at the surface, especially in conjunction with horizontal tectonic loading. The complexity and frictional properties of faults are also relevant. The greatest variability of the stress field arises across the different sedimentary units. Stress magnitudes and stress anisotropy are much larger in stiffer formations such as massive limestones than in softer argillaceous formations. The stiffer formations essentially carry the load of the far-field forces and are therefore more sensitive to changes of the boundary conditions. This general characteristic of stress distribution in the stiff and soft formations is broadly maintained also with progressive loading towards the plastic limit. The stress field in argillaceous sediments within a stack of formations with strongly contrasting mechanical properties like in the Alpine foreland appears to be relatively insensitive to changes in the tectonic boundary conditions and is largely controlled by the maximum stiffness contrast with respect to the load-bearing formations.

Stress field sensitivity analysis in a sedimentary sequence

T. Hergert et al.

Title Page

Abstract

Introduction

Conclusions

References

Tables

Figures



Back

Close

Full Screen / Esc

Printer-friendly Version

Interactive Discussion



1 Introduction

Knowledge of the in situ stress in the subsurface and its local variability is a critical issue for academic questions and application in industry likewise (Fuchs and Müller, 2001; Hergert and Heidbach, 2011; Tingay et al., 2005). In particular for geotechnical projects such as tunnelling, boreholes or reservoir management knowledge of the stress state is required in order to plan safe and sustainable underground operations (Altmann et al., 2014; Moeck et al., 2009; Zoback, 2010).

The stress field in the upper crust can vary strongly on a local scale due to topography, faults and variable properties of formations. Savage and Morin (2002) showed that topography can cause a highly variable stress field up to polarity reversals of the principal stresses. Examples for stress perturbations due to faults have been compiled by Barton and Zoback (1994) and Yale (2003). Warpinski (1989) showed on the basis of a large number of hydraulic fracturing data that linear interpolation of stress magnitudes across different lithologies can result in erroneous estimates. Using a 2-D generic numerical geomechanical model Roche et al. (2013) showed that the impact of formations on the stress field can be significant. This is also shown by Gunzburger and Magnenet (2014) who used stress data to invert the mechanical properties of weak layers in the sediment layers of the Paris basin.

Constraining the stress field at local scale in Northern Switzerland is of particular interest for the evaluation of identified potential geological siting areas in the context of radioactive waste disposal (Nagra, 2008). The siting areas are characterized by moderate local topography (approximately up to 300 to 400 m of difference in relief). The candidate host rocks are Mesozoic argillaceous sediments, which alternate with Mesozoic clastics, marls, carbonates, and evaporites. For high-level waste, the Lower Dogger Opalinus Clay is the anticipated host rock.

Information on the stress field is often very sparse and incomplete, especially at depths relevant for energy resources or subsurface constructions (i.e. a few hundred meters to kilometres). Stress magnitude data for these depths is available in excep-

SED

7, 711–756, 2015

Stress field sensitivity analysis in a sedimentary sequence

T. Hergert et al.

Title Page

Abstract

Introduction

Conclusions

References

Tables

Figures



Back

Close

Full Screen / Esc

Printer-friendly Version

Interactive Discussion



structures in the area which accommodated the south–north directed shortening are the Siglistorf Anticline (SA) and the Stadel–Irchel Anticline (SIA) (Fig. 2). Shortening is much more significant along the Jura fold-and-thrust belt to the southwest of the model area. The formation of the SIA appears to be closely related to the Baden–Irchel–Herdern lineament (BIH), a Pre-Cenozoic fault structure which is also considered to represent the southern boundary of the ENE–WSW striking Permo-Carboniferous Trough system.

The Weiach borehole (Matter et al., 1988) is located roughly in the centre of the model (Fig. 2) and the only direct source of stress information at greater depth. From analysis of borehole breakouts to a depth of approximately 2500 m below ground level the S_H orientation was interpreted to strike approximately 172° N (Heidbach and Reinecker, 2013), which is in good agreement with the findings in regional wells (Fig. 1a). Over a much shorter interval limited to the Upper Dogger and Lower Malm sections at the Weiach borehole, the S_H azimuth was found to deviate from the dominant value in the Mesozoic and Paleozoic formations, striking at 134° N.

The eastern and western model boundaries are oriented 170° N (Fig. 2), which is approximately parallel to the dominant interpreted orientation of S_H and approximately perpendicular to the ENE–WSW trending major fault structures. The top of the model is the topography and the base of the model is at 2500 m below sea level.

2.3 Model assumptions and workflow

Figure 3 gives an overview of the model setup and workflow. The model includes structural information such as geometries of faults and lithological horizons. Ten individual formations are considered which are characterized by their respective rock properties (density, elastic and plastic parameters; Table 1). Each geomechanical formation is considered as homogeneous with isotropic mechanical properties. Fault strength is controlled by the coefficient of friction. An initial stress state representing a reference stress state is established using semi-empirical relationships between the vertical to horizontal stress ratio and the overconsolidation ratio (OCR) of argillaceous

SED

7, 711–756, 2015

Stress field sensitivity analysis in a sedimentary sequence

T. Hergert et al.

Title Page

Abstract

Introduction

Conclusions

References

Tables

Figures

◀

▶

◀

▶

Back

Close

Full Screen / Esc

Printer-friendly Version

Interactive Discussion



2.5 Initial stress state, gravity, boundary conditions and model calibration

2.5.1 Definition of initial stress

The initial stress state of the model considers no horizontal tectonic loading and is in equilibrium with gravity forces. For normally consolidated clays or clay-rich soils, the horizontal to vertical effective stress ratio (K') is generally approximated by $S'_h/S'_V \approx 1 - \sin(\phi')$ (Jáky, 1944), where S'_V is the vertical stress and ϕ' is the effective friction angle. Empirical correlations have shown that the ratio K' of overconsolidated clays or shales during unloading (e.g. exhumation) are elevated with respect to values at identical depth during initial or normal loading (e.g. Brooker and Ireland, 1965). Mayne and Kulhawy (1982) suggested to extend the stress ratio relationship for normally consolidated clays to overconsolidated clays or shales by taking into account the overconsolidation ratio (OCR), such that the effective stress ratio K' becomes

$$K' = (1 - \sin \phi') \cdot \text{OCR}^{\sin \phi'} \quad (1)$$

where OCR is the ratio of the maximum effective overburden stress experienced during its geologic history (S'_{VC}) and the present effective overburden stress (S'_V). S'_{VC} can be estimated e.g. by one-dimensional compression tests.

Applying Eq. (1) to Opalinus Clay by using $\phi' = 25^\circ$ and OCR values from three locations in northern Switzerland sampled at different depths, the depth-dependent effective stress ratio K' may then be approximated as (Giger and Marschall, 2014)

$$K' = 0.58 \cdot \left(1 + \frac{650}{z}\right)^{0.42} \quad (2)$$

where z is the present depth in metres (Fig. 5a). Note, that this relationship represents a depth-trend of effective stress ratios for a situation *without* any horizontal tectonic forces assuming validity of the semi-empirical approach formulated in Eq. (1). Since

SED

7, 711–756, 2015

Stress field sensitivity analysis in a sedimentary sequence

T. Hergert et al.

Title Page

Abstract

Introduction

Conclusions

References

Tables

Figures

◀

▶

◀

▶

Back

Close

Full Screen / Esc

Printer-friendly Version

Interactive Discussion



the numerical geomechanical model of this study uses total stress values, the effective stress ratio K' has to be converted into the total stress ratio K by

$$K = \frac{K'(S_V - P_P) + P_P}{S_V} \quad (3)$$

where S_V is the vertical stress. Assuming hydrostatic pore fluid pressure (P_P) and a constant density of $\rho = 2.5 \text{ g cm}^{-3}$, Eq. (3) simplifies to

$$K = 0.6 \cdot K' + 0.4. \quad (4)$$

The resulting line in Fig. 5b represents the total stress ratio K for the calibration of the initial stress state in Opalinus Clay for the model. Also indicated in the same figure are stress ratios from hydraulic fracturing data from the Opalinus Clay in the boreholes of Benken (Nagra, 2001) and Schlattingen (Klee, 2012) in Northern Switzerland (see Fig. 1 for location). The hydraulic fracturing data represent the in situ stress, i.e. the stress state *including* tectonic loading. K ratios from the S_h and S_H magnitudes at the Benken site plot to the right of the line, indicating that tectonic loading has led to horizontal stresses which are greater than expected by simple burial and unloading from the empirical relationship. Conversely, the K ratio from the S_h magnitude from the Schlattingen well plots to the left of the line, indicating that tectonic unloading may have decreased the expected magnitude from the empirical relationship. This is consistent with the tectonic setting, as the Schlattingen well was drilled east of the Benken well and closer to the Hegau–Bodensee Graben (Nagra, 2014a).

2.5.2 Implementation of initial stress

Technically, the initial state of stress in the model is established by application of gravity on the model volume with its boundaries at the bottom and at the sides being fixed for displacements perpendicular to the model boundaries. During uniaxial compaction, the Poisson's ratio controls the horizontal stress and this mechanism is used to establish

Stress field sensitivity analysis in a sedimentary sequence

T. Hergert et al.

Title Page

Abstract

Introduction

Conclusions

References

Tables

Figures

◀

▶

◀

▶

Back

Close

Full Screen / Esc

Printer-friendly Version

Interactive Discussion



theoretical value that assumes no stress perturbations from faults (Figs. 6 and 7c). The other profile located 2000 m further south between the SA and the SIA seems to be widely unaffected by these faults. Here, the Opalinus Clay is at ~ 800 m depth and K should be 0.845 according to Eq. (4). At this site, good agreement is obtained between the modelled and theoretical K ratio.

2.5.3 Final stress state and displacement boundary conditions

After the initial stress state of the model is established and in equilibrium with gravity, horizontal displacement boundary conditions are applied at the vertical boundaries of the model to incorporate the tectonic stresses that result from the far field forces and from the geological history (Fig. 8). These boundary conditions cannot be derived from geodetic observations as the interpreted displacement rates are very small and uncertainties large (Nagra, 2008). Thus, in order to integrate the available knowledge of south–north compression in the course of the Alpine orogenesis, the model is basically shortened in south–north direction and dilated in east–west direction (Fig. 8). To calibrate the amount of displacement, we fit the observed S_H orientation from the Weiach well (Heidbach and Reinecker, 2013), the overall transtensional tectonic stress regime in Northern Switzerland (Heidbach and Reinecker, 2013) and the measured stress ratio $K = S_h/S_v = 0.94$ from hydraulic fracturing in Opalinus Clay in the nearby Benken well (Nagra, 2001). For the latter value it is assumed that the stress magnitude at the level of the Opalinus Clay at the Benken borehole is a good proxy for the model area some 10 km to the south–west of this location.

The best-fit boundary conditions are displacement of 9 m to the north at the southern model boundary perpendicular to it, while the boundaries in the west and east are pulled by 0.4 m each to the west and east, respectively; the northern model boundary is fixed for displacements perpendicular to the boundary. Displacements parallel to the model boundaries are allowed everywhere. Displacements at the bottom of the model are not allowed in vertical direction while horizontal displacements are permitted. The surface of the model is unconstrained. Due to the slightly rotated boundaries of the

Stress field sensitivity analysis in a sedimentary sequence

T. Hergert et al.

Title Page

Abstract

Introduction

Conclusions

References

Tables

Figures

⏪

⏩

◀

▶

Back

Close

Full Screen / Esc

Printer-friendly Version

Interactive Discussion



From earthquake focal mechanisms the dominant stress regime in the broader region is strike-slip to normal faulting. For the 1999 $M = 3.1$ earthquake near Eglisau at the eastern model boundary at 1–2 km depth a strike-slip focal mechanism solution has been determined (Deichmann et al., 2000; Fig. 1a).

Figure 7 shows the magnitudes of S_h and S_v of the initial and final stress states, respectively, on a north–south cross section and the K ratio at the two depth profiles at the Weiach well and 2000 m south of it. At Weiach at 600 m true vertical depth the K ratio of the final stress state is $K \cong 0.95$ and at 800 m true vertical depth at the location 2000 m south of the Weiach well $K \cong 0.93$, in agreement with $K = 0.94$ derived from the Benken well data. The S_h magnitude increases from the initial stress to the final stress (Fig. 7a and d), whereas the S_v magnitude is essentially unchanged (Fig. 7b and e). Thus, the K ratio increases due to the horizontal tectonic stresses imposed by the boundary conditions.

3 Results of the base model

3.1 Differential stresses

The competent formations Upper Malm and Middle Muschelkalk are clearly characterised by increased differential stress $S_1 - S_3$ of up to 20 MPa compared to low values in the weaker formations, mostly 4 to 7 MPa in the Opalinus Clay (Fig. 10). The vertical changes of differential stress are therefore very pronounced (factor of about four), whereas within a formation differential stress is rather uniform (factor of about two at most), at least within the deeper formations (Fig. 10). Similarly, the horizontal differential stress $S_H - S_h$ is about 3 to 6 MPa in the Opalinus Clay.

SED

7, 711–756, 2015

Stress field sensitivity analysis in a sedimentary sequence

T. Hergert et al.

Title Page

Abstract

Introduction

Conclusions

References

Tables

Figures

◀

▶

◀

▶

Back

Close

Full Screen / Esc

Printer-friendly Version

Interactive Discussion



3.2 Stress ratio

The ratio S_H/S_h ranges between 1.2 and 1.4 in the Opalinus Clay, except in the NW, where it is higher (Fig. 11 top). In the other (stiffer) formations S_H/S_h is clearly higher. Furthermore, S_H/S_h generally increases towards the surface.

The ratio S_H/S_V exhibits very high values > 2 in the uppermost Molasse formation but strongly decreases to 1.5 and less below the Upper Malm (Fig. 11 middle). The ratio S_H/S_V is about 1 at the base of the model, thus also the ratio S_H/S_V generally increases towards the surface. In the Opalinus Clay S_H/S_V ranges between about 1.1 and 1.3 in most of the model area, with an increase to > 1.3 in a narrow stretch of 1–2 km width south of the SA and north of it (Fig. 11 middle).

The ratio S_h/S_V varies between 0.8 and 1.1 in the Opalinus Clay and is slightly less than 1 in most of the model area (Fig. 11 bottom). Also S_h/S_V increases towards the SA and towards the surface. However, differences in S_h/S_V among the individual Mesozoic formations are smaller than for S_H/S_h and S_H/S_V . All stress ratios S_H/S_h , S_H/S_V and S_h/S_V show reduced values within the Opalinus Clay compared to the stiffer formations above and below (Fig. 11). Further, all stress ratios tend to increase beneath topographic depressions, e.g. below the Rhine valley.

4 Results of model variants

In this section the results of the model variants regarding rock properties as well as fault geometry and fault friction are presented. The changes in these model variants with respect to model BM are listed in Table 2.

4.1 Imprints of topography

To investigate the influence of topography a model with homogeneous mechanical properties (E0 in Table 2) is considered. In such a model, the effect of topography is not concealed by the influence of the different rock properties of the individual forma-

SED

7, 711–756, 2015

Stress field sensitivity analysis in a sedimentary sequence

T. Hergert et al.

Title Page

Abstract

Introduction

Conclusions

References

Tables

Figures

◀

▶

◀

▶

Back

Close

Full Screen / Esc

Printer-friendly Version

Interactive Discussion



tions. The pattern of the topography (see Fig. 2) is reflected in the initial S_H magnitudes (i.e. without displacement boundary conditions) with higher values below elevated areas and relatively low values below topographic depressions (Fig. 12, left column). Gradients of topography become much more expressed once tectonic boundary conditions are applied (Fig. 12, right column). In this case S_H corresponds roughly to the north–south component of stress. The stress magnitude S_H is increased below valleys, particularly below east–west elongated ones, while stress is reduced below ridges. The topographical influence on stress can be traced down to several hundred metres depth. Particularly steep slopes of topography are expressed in the stress pattern. The effect from topographic features of small extent disappears at shallower depth than the stress signature from elevation changes of greater lateral extent.

4.2 Influence of rock properties

An increase or decrease of the Young's moduli for the Keuper and Upper Dogger formations below and above the Opalinus Clay, respectively, has only very small impact on the stress ratios S_H/S_h , S_h/S_V and S_H/S_V in the Opalinus Clay. Increasing the Young's modulus of the Keuper and Upper Dogger by 33 % to 20 GPa results in slightly increased stress ratios in the Opalinus Clay, whereas a smaller Young's modulus of the Keuper and the Upper Dogger (33 % less to 10 GPa) results in slightly lower stress ratios in the Opalinus Clay. However, changes in stress ratios are always smaller than 0.1. Figure 13 reveals the strong influence of the variable properties of the individual formations on the stress state by comparison of BM with the homogeneous model E0. Plastic rock behaviour does not result in any significant changes of stress ratios compared to an elastic model. This is because the compressive strength of the rock is not reached throughout most of the model volume. Plastic strain only occurs at some locations at the bottom or at the edges of the model and where the edges of the model are intersected by faults.

Stress field sensitivity analysis in a sedimentary sequence

T. Hergert et al.

Title Page

Abstract

Introduction

Conclusions

References

Tables

Figures

⏪

⏩

◀

▶

Back

Close

Full Screen / Esc

Printer-friendly Version

Interactive Discussion



4.3 Influence of fault geometry and coefficient of friction

In model G10 the effective coefficient of friction on the faults is set to $\mu' = 1.0$ (Table 2). The results (Fig. 14) show an overall increase of the ratios S_H/S_h and S_H/S_V , but a decreased ratio of S_h/S_V in the Opalinus Clay. An exception is in the western and southern part of the block between SIA and SA, where S_h/S_V increases. Changes are smaller than 0.1 in most of the model area and 0.2 south of the SA in the eastern half of the model. From about half a kilometre north of the SA to about 2 km south of the SA, S_H/S_h increases by about 50 % in the Upper Malm (S_H/S_h up to 2.5) compared to BM. The ratio S_H/S_h increases also south of it, although less.

In the model variant GB faults are deactivated below the base of the Middle Muschelkalk by using a very high coefficient of friction ($\mu' = 100$), which means that faults essentially become locked. This reduces the stress ratios S_H/S_h , S_h/S_V and S_H/S_V within the Opalinus Clay in most of the model area, particularly immediately south of the SA (Fig. 14). However, changes with respect to BM are smaller than 0.1. Below the Opalinus Clay the stress ratios increase.

Incorporation of a back thrust adjacent to the SA (Model GR in Fig. 14) reduces the horizontal stresses outside the wedge formed by the back thrust and the SA. The decrease of the stress ratios S_H/S_h , S_h/S_V and S_H/S_V within the Opalinus Clay compared to BM occurs predominantly close to the wedge. The decreased ratios are also found north of the wedge. The uplift of the wedge lowers horizontal stress in the individual formations. In the Opalinus Clay the effect of the back thrust is smaller than at shallower depth because the wedge terminates just below the Opalinus Clay. Particularly, horizontal stress anisotropy is reduced by the back thrust in the Upper Malm south of the SA.

4.4 Plastic limit

In the previous model runs the southern model boundary was displaced by 9 m to the north to account for the tectonic boundary conditions, i.e. to generate the desired

SED

7, 711–756, 2015

Stress field sensitivity analysis in a sedimentary sequence

T. Hergert et al.

Title Page

Abstract

Introduction

Conclusions

References

Tables

Figures

◀

▶

◀

▶

Back

Close

Full Screen / Esc

Printer-friendly Version

Interactive Discussion



horizontal in situ stress magnitudes. This rather moderate amount of shortening did not lead to any significant failure of the geomechanical units since the compressive strength is not reached. In this section the effect of further south–north shortening is assessed by starting with model BM and sequentially adding up to 21 m of additional shortening (total 30 m) and allowing for additional extension both at the western and eastern model boundaries up to 1.1 m each (total 3 m). Assuming that the overall south–north shortening between the central Alps and the southern Black Forest north of the geological siting area is between 0.1 and 1 mm a⁻¹, the south–north shortening within the model area is approximately between 0.01 and 0.1 mm a⁻¹. Thus, 21 m of additional shortening may broadly represent a time span between 2.1 Ma and 210 ka. The real south–north shortening is still not resolved in the GPS data.

The evolution of differential stress with progressive shortening (left column of Fig. 15) shows that the stiff formations of the Upper Malm and the Upper Muschelkalk bear most of the differential stress accumulation. The maximum values of horizontal differential stress $S_H - S_h$ in the Opalinus Clay is < 20 MPa whereas in the stiffer formations it is partly > 60 MPa. In order to assess which of the formations will most likely undergo plastic deformation at additional shortening the fracture potential $FP = \sigma_d / \sigma_{d,crit}$ is calculated for each unit using the values for the friction angle and the cohesion given in Table 1 (σ_d is the differential stress and $\sigma_{d,crit}$ the critical differential stress at which the failure envelope is reached). Thus, plastification occurs for $FP \geq 1$. The results show that this plastic limit is only reached after approximately 15 m of additional shortening when the FP value reaches values close to or equal to one (right column of Fig. 15). The Molasse sediments and the stiff formations that are close to the surface are most prone to failure. In the Opalinus Clay FP values are below 0.8 except near the SA where FP values are close to one at the final stage of 21 m additional south–north shortening. The stiff Upper Muschelkalk below the Opalinus Clay has even slightly lower FP values compared to the clay-rich units.

Stress field sensitivity analysis in a sedimentary sequence

T. Hergert et al.

[Title Page](#)[Abstract](#)[Introduction](#)[Conclusions](#)[References](#)[Tables](#)[Figures](#)[◀](#)[▶](#)[◀](#)[▶](#)[Back](#)[Close](#)[Full Screen / Esc](#)[Printer-friendly Version](#)[Interactive Discussion](#)

Stress field sensitivity analysis in a sedimentary sequence

T. Hergert et al.

Title Page

Abstract

Introduction

Conclusions

References

Tables

Figures

◀

▶

◀

▶

Back

Close

Full Screen / Esc

Printer-friendly Version

Interactive Discussion



the competent formations than in the weak formations. It is interpreted that the northward directed horizontal push is carried predominantly by the formations with higher stiffness. The stiff Upper Malm and Middle Muschelkalk formations above and below the argillaceous formations shield those weaker formations, leaving them in a stress shadow. The strong variability of stress over different formations implies that derivation of linear depth gradients of stress based on a few measurements may be misleading.

Moderate stiffness variation of the Upper Dogger and Upper Keuper formations resting above and below the Opalinus Clay affects stress ratios in the Opalinus Clay only marginally. This is because the yet stiffer Upper Malm and Middle Muschelkalk exert a dominant control as load-bearing formations. The very uniform S_H orientation over all formations indicates relatively high horizontal differential stress. This does not imply, however, that there is no stress decoupling active in any of the formations, because the boundary conditions are uniformly applied over the whole depth extent of the model.

Variable stress magnitudes in different formations of a sedimentary sequence have been observed in other areas as well (Burlet and Ouvry, 1989; Evans et al., 1989; Plumb et al., 1991; Wileveau et al., 2007). In the model differential stress is lower and S_h magnitudes are higher in the argillaceous formations compared to the stiffer formations (Figs. 9 and 10). Similarly, in the Paris basin Gunzburger and Cornet (2007) have found S_h magnitudes in a clay formation to be higher than in adjacent stiff limestone units from hydraulic fracturing. Based on a compilation of S_h measurements Plumb (1994) found that whether S_h magnitudes were higher in softer or stiffer formations depends on whether the state of the sedimentary basin is relaxed (S_h in soft units higher) or compressed (S_h in stiff units higher). This is qualitatively also reproduced also in Fig. 7f.

5.1.3 Role of faults on stress

The role of the semi-generic east–west striking SA and the SIA fault is revealed by comparing models with different coefficient of friction on the faults. The end member case of infinite friction would mean a fault is absent because a faults' ability to slip is

SED

7, 711–756, 2015

Stress field sensitivity analysis in a sedimentary sequence

T. Hergert et al.

[Title Page](#)[Abstract](#)[Introduction](#)[Conclusions](#)[References](#)[Tables](#)[Figures](#)[◀](#)[▶](#)[◀](#)[▶](#)[Back](#)[Close](#)[Full Screen / Esc](#)[Printer-friendly Version](#)[Interactive Discussion](#)

Below the Mesozoic sediments, it was assumed that there are uniform Permo-Carboniferous sediments down to the model boundary at 2500 m below sea level. Thus, no distinction is made in the model between crystalline and other pre-Mesozoic basement, although in the Weiach well the contact between Permo-Carboniferous sediments and the Pre-Mesozoic basement was encountered at 2020 m depth. The boundaries of the Permo-Carboniferous Trough are not known precisely and it is possible that the thickness of the Permo-Carboniferous sediments varies strongly over the model area and may even be absent at some locations of the area. However, the impact of this heterogeneity on the stress field in the sediments is probably small compared to the local stiffness variability in the Mesozoic sediments.

The boundaries of the model are rather close to the siting area. Therefore, boundary effects might affect the results. This holds particularly for the boundary conditions at the eastern and western model boundaries at the intersections of the faults with the model boundaries. As the SA and SIA are reactivated left- and right-laterally, respectively, the boundaries should be defined accordingly, allowing fault slip at the boundaries. However, once fault slip is defined at the boundaries, fault slip is no longer an independent result of the model and it is unclear what amount of slip should be imposed. In turn, if no boundary-perpendicular fault slip is allowed at the model boundaries, which is the case for the model presented, an artefact comes into the model as artificial east–west compression is generated at the eastern model boundary south of the SA and extension at the western model boundary south of the SA due to the left-lateral displacement at this fault.

The absence of data on stress magnitudes within the model area limits the reliability of the absolute stresses resulting from the model. The assumption made that the reference stress and the tectonic load are the same in Weiach as in Benken, where stress magnitude data are available, is critical. While at Benken the Mesozoic overlies directly the Pre-Mesozoic basement, Weiach is situated over Permo-Carboniferous sediments and possibly experiences an influence of the Permo-Carboniferous Trough.

Fault geometries used in this study are highly simplified. This is considered appropriate for first-order sensitivity studies. More realistic and complex fault geometries would certainly affect the stress field in the vicinity of fault zones.

Remnant stresses from the geological history are difficult to assess and so are an appropriate initial stress and boundary conditions. The reliability of the model results may be increased if more detailed information on the fault geometries would be available, if the interface between the Permo-Carboniferous sediments and the crystalline basement could be better resolved, if details on the deformation occurring in the area could be determined and most of all if information on stress magnitudes were available in representative formations within the siting area Nördlich Lägern.

6 Conclusions

A stress sensitivity analysis using numerical geomechanical modelling was performed to assess the influence of topography, of faults and of mechanical properties on the stress state of a sedimentary sequence in Northern Switzerland. The effect of topography on the state field can be attributed predominantly to the interaction between the relief features and the tectonic loading rather than to the gravitational effect alone. Fault structures affect the local stress field as they tend to reduce horizontal stresses from the far-field. But the greatest variability in the stress field in the sensitivity study stems from the stiffness contrasts in the sedimentary sequence. The stiffer formations (Upper Malm and Upper Muschelkalk) take up the majority of tectonic stresses associated with the far-field push, while differential stresses remain relatively small in the softer argillaceous formations. Hence the in situ stress field in argillaceous sediments within a stack of formations with strongly contrasting mechanical properties like in the Swiss Alpine foreland basin appears to be relatively insensitive to changes in the tectonic boundary conditions and is largely controlled by the maximum stiffness contrast with respect to the load-bearing formations.

Stress field sensitivity analysis in a sedimentary sequence

T. Hergert et al.

Title Page

Abstract

Introduction

Conclusions

References

Tables

Figures

◀

▶

◀

▶

Back

Close

Full Screen / Esc

Printer-friendly Version

Interactive Discussion



Stress field sensitivity analysis in a sedimentary sequence

T. Hergert et al.

Title Page

Abstract

Introduction

Conclusions

References

Tables

Figures

◀

▶

◀

▶

Back

Close

Full Screen / Esc

Printer-friendly Version

Interactive Discussion



Deichmann, N. and Ernst, J.: Earthquake focal mechanisms of the induced seismicity in 2006 and 2007 below Basel (Switzerland), *Swiss J. Geosci.*, 102, 457–466, doi:10.1007/s00015-009-1336-y, 2009.

Deichmann, N., Ballarin Dolfin, D., and Kastrup, U.: Seismizität der Nord- und Zentralschweiz, *Nagra Tech. Ber. NTB 00–05*, p. 113, Nagra, Wettingen, 2000.

Diebold, P. and Noack, T.: Late Palaeozoic troughs and Tertiary structures in the eastern folded Jura, in: *Deep Structure of the Swiss Alps: Results of NRP20*, edited by: Pfiffner, O. A., Lehner, P., Heitzmann, P., Mueller, S., and Steck, A., Birkhäuser Verlag, Basel, 59–63, 1997.

Evans, K. F., Engelder, T., and Plumb, R. A.: Appalachian stress study, 1. A detailed description of in-situ stress variations in Devonian shale of the Appalachian Plateau, *J. Geophys. Res.*, 94, 7129–7154, 1989.

Fischer, K. and Henk, A.: A workflow for building and calibrating 3-D geomechanical models – a case study for a gas reservoir in the North German Basin, *Solid Earth*, 4, 347–355, doi:10.5194/se-4-347-2013, 2013.

Fuchs, K. and Müller, B.: World stress map of the Earth: a key to tectonic processes and technological applications, *Naturwissenschaften*, 88, 357–371, 2001.

Giger, S. and Marschall, P.: Geomechanical properties, rock models and in-situ stress conditions for Opalinus Clay in Northern Switzerland, *Nagra Arbeitsber. NAB 14-01*, 2014.

Griffith, W. A., Becker, J., Cione, K., Miller, T., Pan, E.: 3-D topographic stress perturbations and implications for ground control in underground coal mines, *Int. J. Rock Mech. Min.*, 70, 59–68, doi:10.1016/j.ijrmms.2014.03.013, 2014.

Gunzburger, Y., Cornet, F. H.: Rheological characterization of a sedimentary formation from a stress profile inversion, *Geophys. J. Int.*, 168, 402–418, doi:10.1111/j.1365-246X.2006.03140.x, 2007.

Gunzburger, Y., and Magnenet, V.: Stress inversion and basement-cover stress transmission across weak layers in the Paris basin, France, *Tectonophysics*, 617, 44–57, 2014.

Häring, M. O., Schanz, U., Ladner, F., and Dyer, B. C.: Characterisation of the Basel 1 enhanced geothermal system, *Geothermics*, 37, 469–495, 2008.

Heidbach, O. and Reinecker, J.: Analyse des rezenten Spannungsfeldes der Nordschweiz, *Nagra Arb. Ber. NAB 12-05*, p. 120, Nagra, Wettingen, 2013.

Heidbach, O., Reinecker, J., Tingay, M., Müller, B., Sperner, B., Fuchs, K., and Wenzel, F.: Plate boundary forces are not enough: second- and third-order stress patterns highlighted in the world stress map database, *Tectonics*, 26, TC6014, doi:10.1029/2007TC002133, 2007.

SED

7, 711–756, 2015

**Stress field
sensitivity analysis in
a sedimentary
sequence**

T. Hergert et al.

[Title Page](#)[Abstract](#)[Introduction](#)[Conclusions](#)[References](#)[Tables](#)[Figures](#)[◀](#)[▶](#)[◀](#)[▶](#)[Back](#)[Close](#)[Full Screen / Esc](#)[Printer-friendly Version](#)[Interactive Discussion](#)

- Nagra: Sondierbohrung Benken Untersuchungsbericht, Nagra Tech. Ber. NTB 00-01, p. 273, Nagra, Wettingen, 2001.
- Nagra: Vorschlag geologischer Standortgebiete für das SMA- und das HAA-Lager, Nagra Tech. Ber. NTB 08-04, p. 395, Nagra, Wettingen, 2008.
- 5 Nagra: SGT Etappe 2: Vorschlag weiter zu untersuchender geologischer Standortgebiete mit zugehörigen Standortarealen für die Oberflächenanlage. Geologische Grundlagen, Dossier II. Nagra Tech. Ber. NTB 14-02, 2014a.
- Nagra: SGT Etappe 2: Vorschlag weiter zu untersuchender geologischer Standortgebiete mit zugehörigen Standortarealen für die Oberflächenanlage. Geologische Grundlagen, Dossier
- 10 IV. Nagra Tech. Ber. NTB 14-02, 2014b.
- Pan, E., Amadei, B., and Savage, W. Z.: Gravitational and tectonic stresses in anisotropic rock with irregular topography, *Int. J. Rock Mech. Min.*, 32, 201–214, 1995.
- Plumb, R. A.: Variations of the least horizontal stress magnitude in sedimentary rocks, in: *Proc. 1st North Amer. Rock Mech. Symp.*, Austin, Balkema, Rotterdam, 71–78, 1994.
- 15 Plumb, R. A., Evans, K. F., and Engelder, T.: Geophysikal log responses and their correlation with bed-to-bed stress contrasts in Paleozoic rocks, Appalachian Plateau, NY, *J. Geophys. Res.*, 96, 14509–14528, 1994.
- Reinecker, J., Tingay, M., Müller, B., and Heidbach, O.: Present-day stress orientation in the Molasse Basin, *Tectonophysics*, 462, 1–4, doi:10.1016/j.tecto.2009.1007.1021, 2010.
- 20 Reiter, K. and Heidbach, O.: 3-D geomechanical–numerical model of the contemporary crustal stress state in the Alberta Basin (Canada), *Solid Earth*, 5, 1123–1149, doi:10.5194/se-5-1123-2014, 2014.
- Roche, V., Homberg, C., and Rocher, M.: Fault nucleation, restriction, and aspect ratio in layered sections: quantification of the strength and stiffness roles using numerical modeling, *J. Geophys. Res.*, 118, 1–15, doi:10.1002/jgrb.50279, 2013.
- 25 Saucier, F., Humphreys, E., and Weldon, R.: Stress near geometrically complex strike-slip faults: application to the San Andreas Fault at Cajon Pass, southern California, *J. Geophys. Res.*, 97, 5081–5094, doi:10.1029/91JB02644, 1992.
- Savage, W. Z. and Morin, R. H.: Topographic stress perturbations in southern Davis Mountains, west Texas 1. Polarity reversal of principal stresses, *J. Geophys. Res.*, 107, 2339, doi:10.1029/2001JB000484, 2002.
- 30

Stress field sensitivity analysis in a sedimentary sequence

T. Hergert et al.

Title Page

Abstract

Introduction

Conclusions

References

Tables

Figures

◀

▶

◀

▶

Back

Close

Full Screen / Esc

Printer-friendly Version

Interactive Discussion



Schmitt, D. R., Currie, C. A., and Zhang, L.: Crustal stress determination from boreholes and rock cores: fundamental principles, *Tectonophysics*, 1011–1026 doi:10.1016/j.tecto.2012.1008.1029, 2012.

Simpson, R. W.: Quantifying Anderson's fault types, *J. Geophys. Res.*, 102, 17909–17919, 1997.

Sperner, B., Müller, B., Heidbach, O., Delvaux, D., Reinecker, J., and Fuchs, K.: Tectonic stress in the Earth's crust: advances in the world stress map project, in: *New Insights in Structural Interpretation and Modelling*, Volume 212, edited by: Nieuwland, D. A., Geological Society, London, 101–116, 2003.

Tingay, M., Müller, B., Reinecker, J., Heidbach, O., Wenzel, F., and Fleckenstein, P.: Understanding Tectonic Stress in the Oil Patch: The World Stress Map Project, *The Leading Edge*, 1276–1282, 2005.

Valley, B. and Evans, K. F.: Estimation of the stress magnitudes in Basel enhanced geothermal system, in: *Proceedings World Geothermal Congress, Melbourne, Australia, 19–25 April 2015*, 2015.

Warpinski, N. R.: Determining the minimum in situ stress from hydraulic fracturing through perforations, *Int. J. Rock Mech. Min.*, 26, 523–531, 1989.

Warpinski, N. R. and Teufel, L. W.: In-situ stress measurements at Rainier Mesa, Nevada Test Site – influence of topography and lithology on the stress state in tuff, *Int. J. Rock Mech. Min.*, 28, 143–161, 1991.

Wileveau, Y., Cornet, F. H., Desroches, J., and Blumling, P.: Complete in situ stress determination in an argillite sedimentary formation, *Phys. Chem. Earth*, 32, 866–878, 2007.

Yale, D. P.: Fault and stress magnitude controls on variations in the orientation of in situ stress, *Geol. Soc. Spec. Publ.*, 209, 55–64, doi:10.1144/GSL.SP.2003.209.01.06, 2003.

Zang, A. and Stephansson, O.: *Stress in the Earth's Crust*, Springer, Heidelberg, 323 p., 2010.

Ziegler, P. and Dèzes, P.: Crustal evolution of Western and Central Europe, in: *European Lithosphere Dynamics*, Volume 32, edited by: Gee, D. G. and Stephenson, R. A., *Geol. Soc. Mem.*, London, doi:10.1144/GSL.MEM.2006.1032.1101.1103, 1143–1156, 2006.

Zoback, M.: *Reservoir Geomechanics*, Cambridge, Cambridge, 449 p., 2010.

Zoback, M. L.: First and second order patterns of stress in the lithosphere: the world stress map project, *J. Geophys. Res.*, 97, 11703–11728, 1992.

Stress field sensitivity analysis in a sedimentary sequence

T. Hergert et al.

Table 2. Properties of the model variants (only changes with respect to the base model BM are listed).

Model	Properties	effective friction coefficient μ'	boundary conditions
BM	see Table 1	0.2	NS: 9 m EW: –0.8 m (total E+W)
E0	$\rho = 2.6 \text{ g cm}^{-3}$, $\nu = 0.26$, $E = 25 \text{ GPa}$ in all formations		
E1	Upper Dogger: $E = 20 \text{ GPa}$ Lias and Upper Keuper: $E = 20 \text{ GPa}$		
E2	Upper Dogger: $E = 20 \text{ GPa}$ Lias and Upper Keuper: $E = 10 \text{ GPa}$		
E3	Upper Dogger: $E = 10 \text{ GPa}$ Lias and Upper Keuper: $E = 20 \text{ GPa}$		
E4	Upper Dogger: $E = 10 \text{ GPa}$ Lias and Upper Keuper: $E = 10 \text{ GPa}$		
G10		1.0	
GB		0.2 (sediments), 100 (basement)	
GR		0.2 (incl. generic back thrust)	
P2			NS: 30 m EW: –1.5 (gradually)

Title Page

Abstract

Introduction

Conclusions

References

Tables

Figures

◀

▶

◀

▶

Back

Close

Full Screen / Esc

Printer-friendly Version

Interactive Discussion



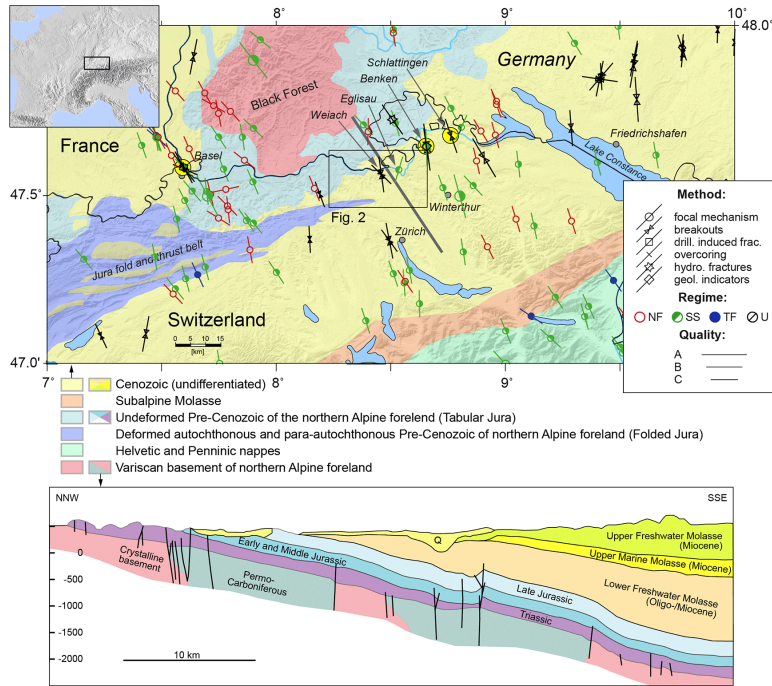


Figure 1. General geological setting of the model area in Northern Switzerland. Top: main geological units (after Nagra, 2008) and 128 A–C quality data records of the revised World Stress Map database release 2008 (Heidbach and Reinecker, 2013; Heidbach et al., 2008). Bars indicate orientation of maximum horizontal stress S_H , symbols indicate type of stress indicator and colours relate to tectonic regime with red for normal faulting (NF), green for strike-slip faulting (SS), blue for thrust faulting (TF), and black for unknown tectonic regime (U). Yellow circles show the three locations where stress magnitude data are available (Basel, Benken, Schlattingen). Black line denotes the location of the cross section below. Bottom: generalized cross section through the main lithological layers in the northern Alpine foreland modified after Mazurek et al. (2006).

Stress field sensitivity analysis in a sedimentary sequence

T. Hergert et al.

Title Page

Abstract

Introduction

Conclusions

References

Tables

Figures

◀

▶

◀

▶

Back

Close

Full Screen / Esc

Printer-friendly Version

Interactive Discussion



Stress field sensitivity analysis in a sedimentary sequence

T. Hergert et al.

Title Page

Abstract

Introduction

Conclusions

References

Tables

Figures

◀

▶

◀

▶

Back

Close

Full Screen / Esc

Printer-friendly Version

Interactive Discussion

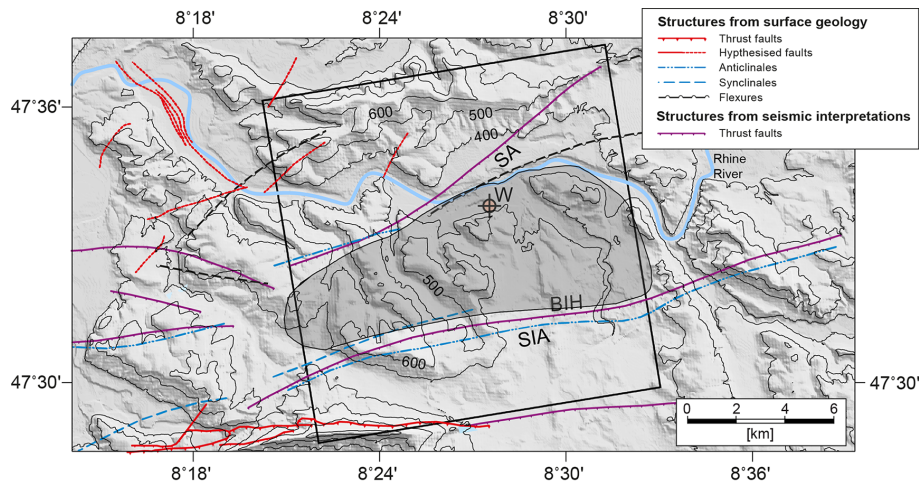


Figure 2. Tectonic map showing the location and extent of the model area (14 km × 14 km, black square). The Stadel–Irchel Anticline (SIA) and the Siglistorf Anticline (SA) are implemented in the model; the Baden–Irchel Herdern Lineament (BIH) is presumably coincident with the SIA at depth. The Weiach well (W) is indicated within the siting area Nördlich Lägern (grey shaded area). Topography contours (thin black lines) in m a.s.l.; note the variation of elevation of approximately 300 m within the model area. After Nagra (2008).

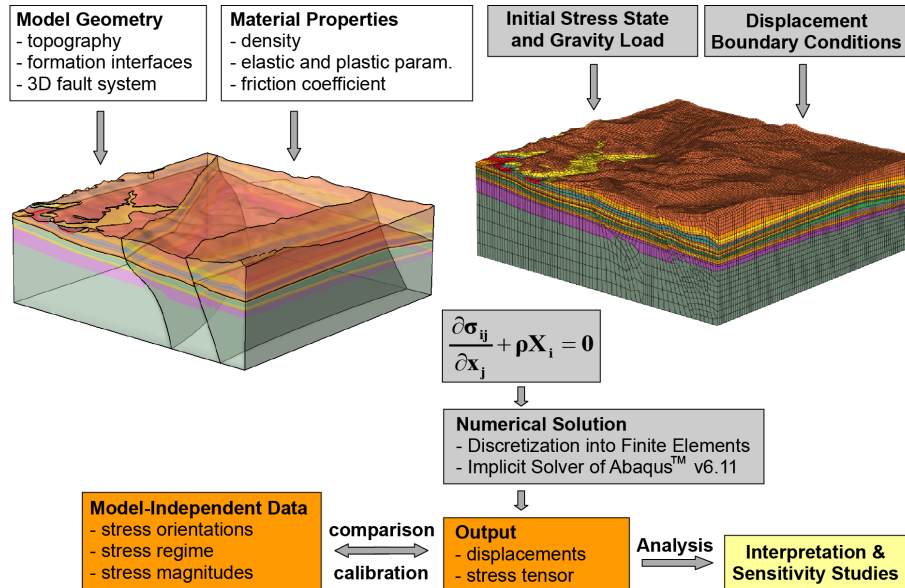


Figure 3. General workflow. Left figure: 3-D view of the model structure. Right figure: discretised model volume. White boxes: assembly of model geometry, rock properties and the 3-D fault system. Grey boxes: gravity, initial stress field and displacement boundary conditions are determined and applied; numerical solution. The partial differential equations of the equilibrium of forces in 3-D are solved using the finite element method (σ_{ij} stress tensor, x_j Cartesian coordinates, ρ density, and X_i body forces). Orange boxes: model results are compared to model-independent data. Yellow box: once the fit to the model-independent observations is acceptable the model results are interpreted and analysed. This includes a sensitivity analysis with respect to the uncertainties of the model parameters.

Stress field sensitivity analysis in a sedimentary sequence

T. Hergert et al.

Title Page

Abstract Introduction

Conclusions References

Tables Figures

◀ ▶

◀ ▶

Back Close

Full Screen / Esc

Printer-friendly Version

Interactive Discussion



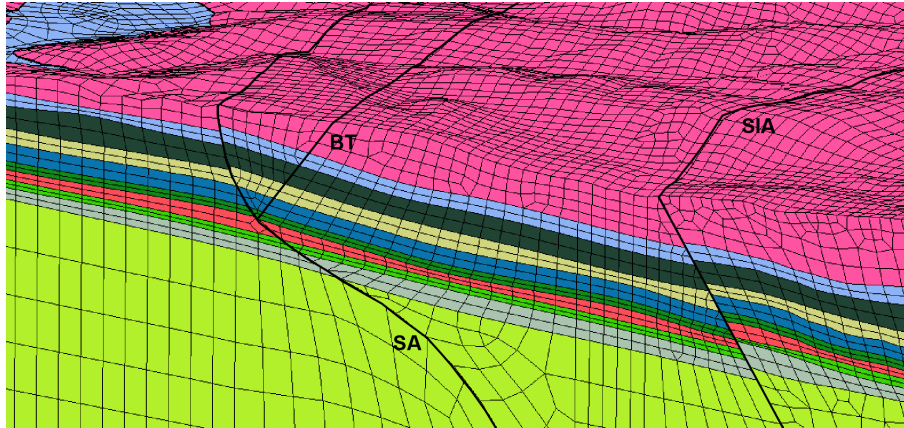


Figure 4. Discretised model volume viewed from south-west. Thick black lines indicate the faults that are implemented as contact surfaces with Coulomb friction. Color-coded are the individual geomechanical units.

**Stress field
sensitivity analysis in
a sedimentary
sequence**

T. Hergert et al.

Title Page

Abstract Introduction

Conclusions References

Tables Figures

◀ ▶

◀ ▶

Back Close

Full Screen / Esc

Printer-friendly Version

Interactive Discussion



Stress field sensitivity analysis in a sedimentary sequence

T. Hergert et al.

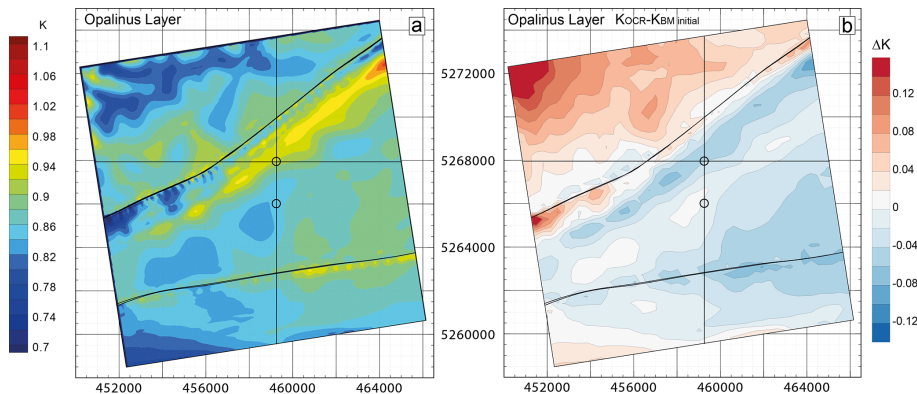


Figure 6. Initial stress state of the model at the centre of the Opalinus Clay formation (i.e. stress state without tectonic loading). **(a)** $K = S_h/S_v$ of the initial stress. **(b)** Difference between the theoretical K ratio from Eq. (4) and the initial stress state in the model as shown in **(a)**. Small circles indicate the location of the two depth profiles displayed in c and f, the northern of which is the location of the Weiach well.

Stress field sensitivity analysis in a sedimentary sequence

T. Hergert et al.

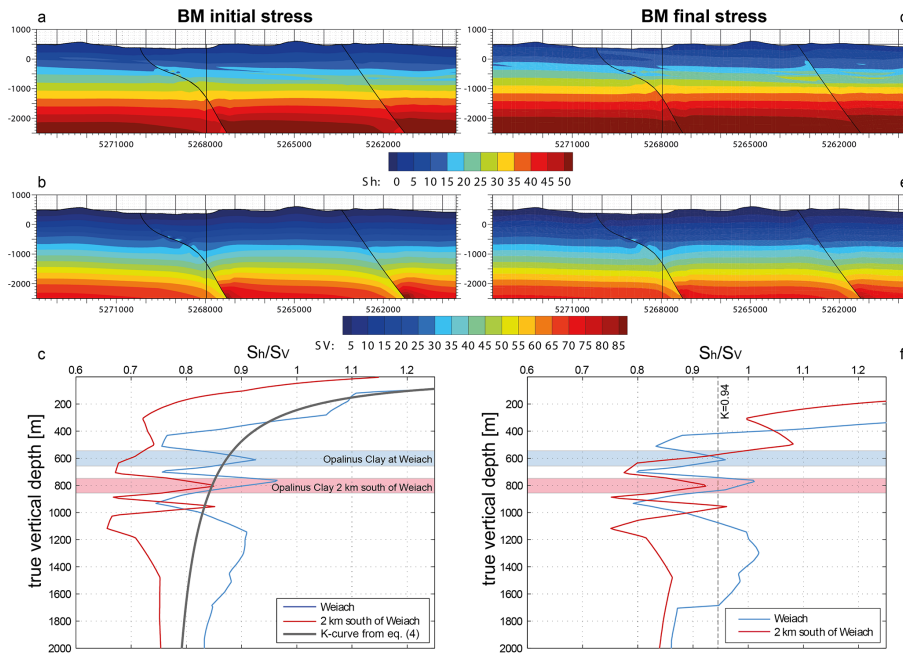


Figure 7. Magnitude of S_h (first row) and S_v (second row) on a north–south cross section through the Weiach well and $K = S_h/S_v$ on depth profiles at the location of the Weiach well and 2000 m south of it (third row) of initial (left column) and final stress (right column) of the base model BM. Note, that initial stress state is without tectonic boundary conditions and final stress state with tectonic boundary conditions applied. The grey line on the lower left figure corresponds to the line in Fig. 5b, i.e. Eq. (4). Dashed line in (f) marks the value $K = 0.94$, which is derived from hydraulic fracturing data at the Benken well in Opalinus Clay at a depth of 630 m.

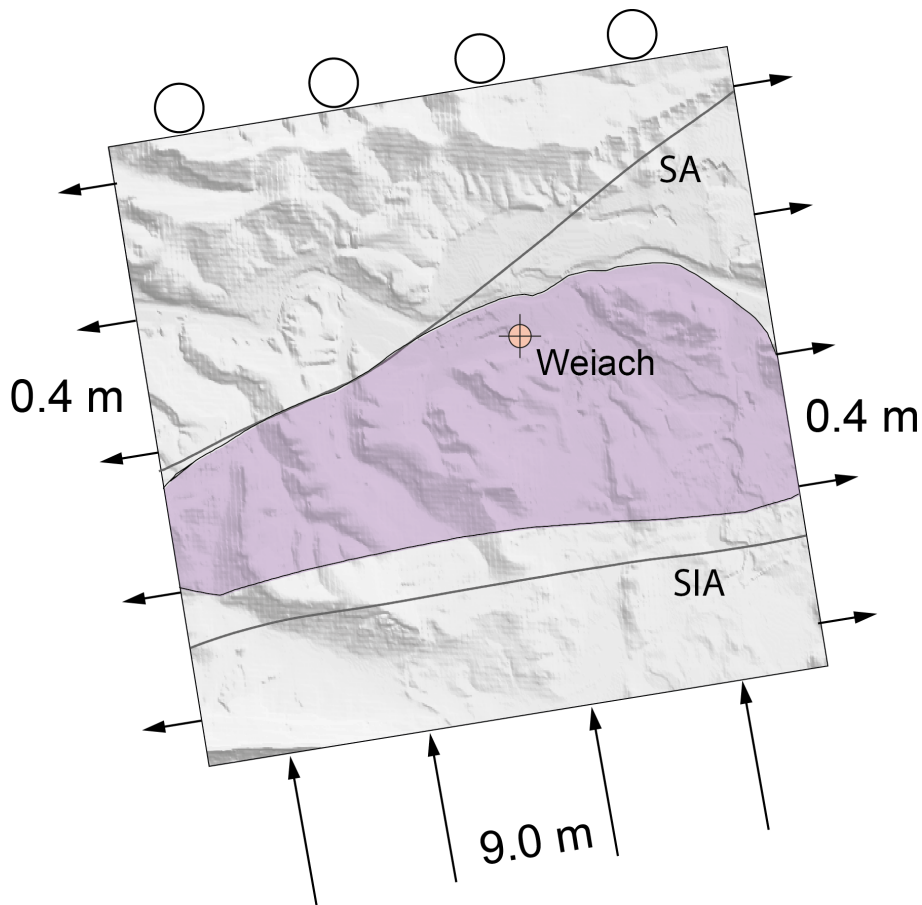


Figure 8. Displacement boundary conditions of Model BM. Circles at the northern model boundary denote that no displacement perpendicular to the boundary is allowed, but parallel to it. Thin lines indicate the two implemented faults SA and SIA; purple area shows the extent of the siting area Nördlich Lägern.

**Stress field
sensitivity analysis in
a sedimentary
sequence**

T. Hergert et al.

Title Page

Abstract

Introduction

Conclusions

References

Tables

Figures

◀

▶

◀

▶

Back

Close

Full Screen / Esc

Printer-friendly Version

Interactive Discussion



Stress field sensitivity analysis in a sedimentary sequence

T. Hergert et al.

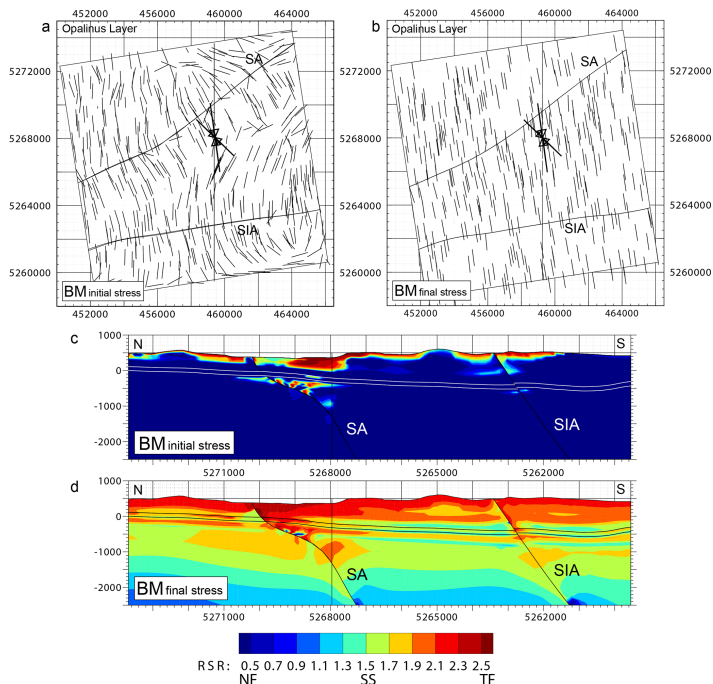


Figure 9. S_H orientation and tectonic regime. **(a)** S_H orientation at the centre of the Opalinus Clay layer for the initial stress field of model BM. Thin black lines show the modelled S_H orientations and the two thick black lines the S_H orientation derived at two depth levels at the Weiach well by Heidbach and Reinecker (2013) (see also Fig. 1). Thin north–south oriented line denotes location of the cross sections in **(c)** and **(d)**. **(b)** Same as **(a)** but for final stress field of model BM after applying tectonic loading. **(c)** Tectonic regime in terms of Regime Stress Ratio (RSR) on a north–south cross section through the Weiach well for the initial stress field of model BM. The RSR provides a continuous range of the tectonic regime with NF = Normal Faulting, SS = Strike–Slip, TF = Thrust Faulting. **(d)** Same as in **(c)** but for the final stress state of model BM. The south dipping Opalinus Clay is indicated by thin black and white lines, respectively.

Stress field sensitivity analysis in a sedimentary sequence

T. Hergert et al.

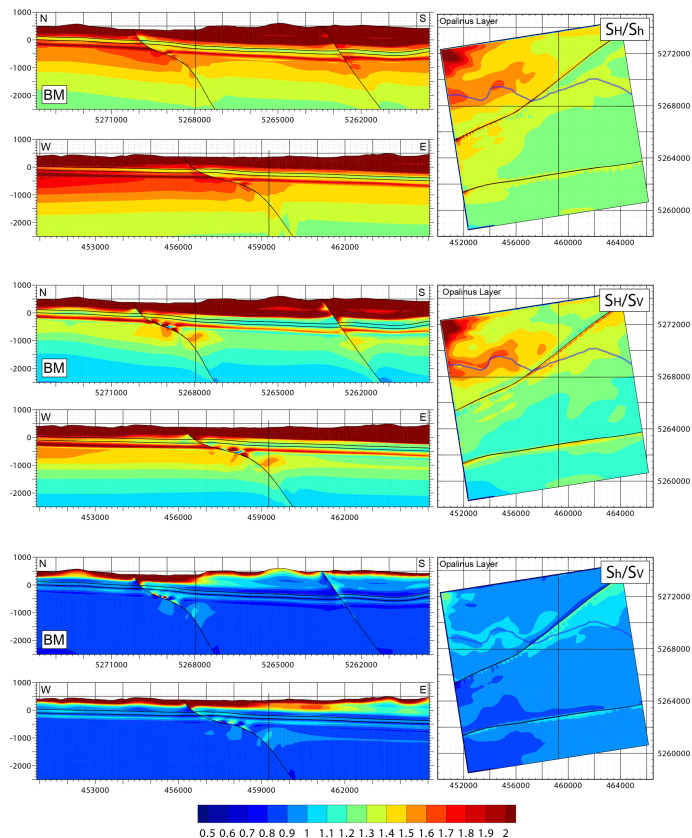


Figure 11. Stress ratios S_H/S_h (top), S_H/S_V (middle) and S_h/S_V (bottom) in north–south and east–west cross sections through the Weiach well (left) and in the centre of the Opalinus Clay formation (right). Colour scale is the same for all figures. Thin lines denote location of cross sections, faults and top and bottom of the Opalinus Clay formation. Blue line on the maps views on the right indicates the location of the Rhine River.

Stress field sensitivity analysis in a sedimentary sequence

T. Hergert et al.

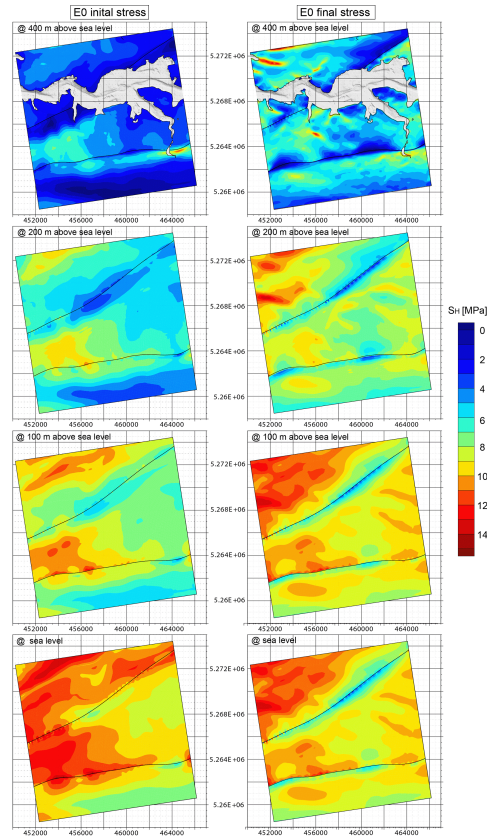


Figure 12. S_H magnitude from the homogeneous model (E0) at different elevations with respect to sea level. Left column without displacement boundary conditions, right column with displacement boundary conditions applied.

Stress field sensitivity analysis in a sedimentary sequence

T. Hergert et al.

Title Page

Abstract

Introduction

Conclusions

References

Tables

Figures

◀

▶

◀

▶

Back

Close

Full Screen / Esc

Printer-friendly Version

Interactive Discussion

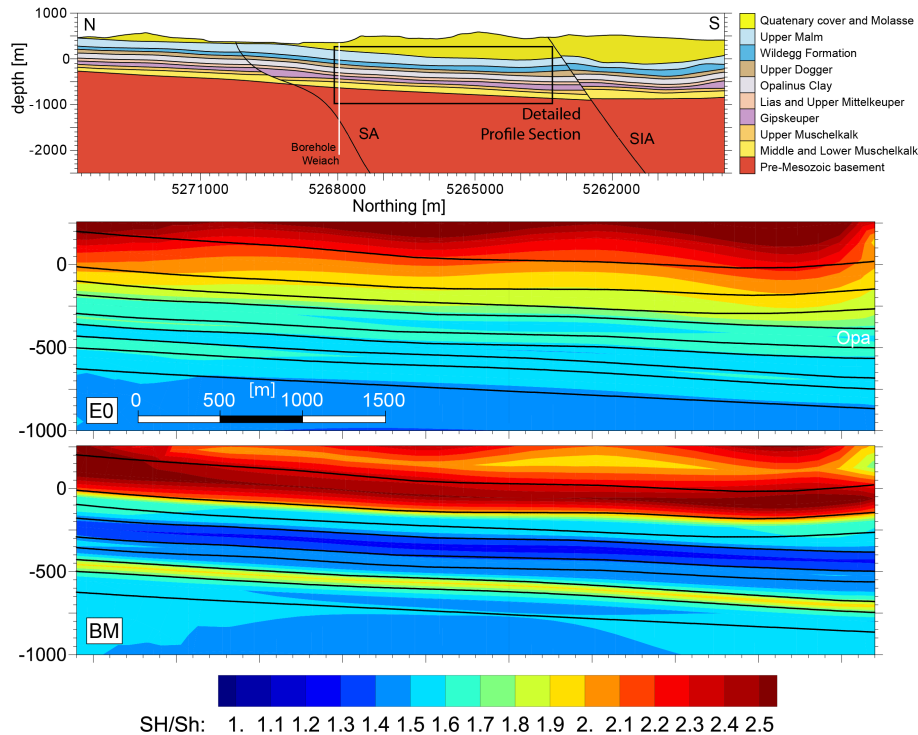


Figure 13. Detailed view of S_H/S_h ratio in north–south cross sections through the Weiach well for different Young’s moduli. Geomechanical stratification for reference (top), homogeneous model E0 (middle) and base model BM (bottom) with rock properties as defined in Table 1.

SED

7, 711–756, 2015

Stress field sensitivity analysis in a sedimentary sequence

T. Hergert et al.

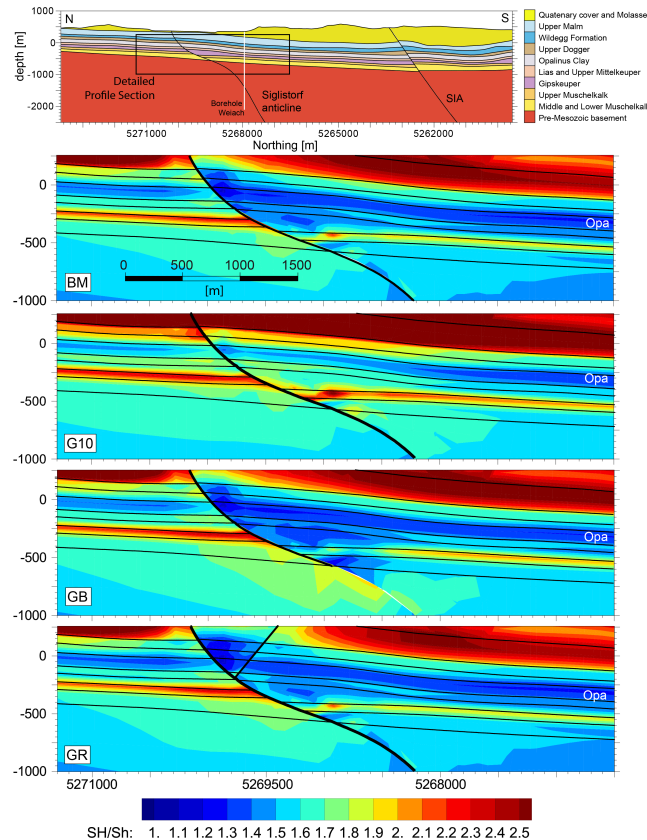


Figure 14. S_H/S_h in north–south cross section through the Weiach well for different fault geometries. BM is the base model, G10 the model with $\mu' = 1.0$, GB the model where the SA is inactive in the pre-Mesozoic basement and GR the model with a generic back thrust. Box in the upper figure shows location of the sections.

Title Page

Abstract Introduction

Conclusions References

Tables Figures

◀ ▶

◀ ▶

Back Close

Full Screen / Esc

Printer-friendly Version

Interactive Discussion



Stress field sensitivity analysis in a sedimentary sequence

T. Hergert et al.

Title Page

Abstract

Introduction

Conclusions

References

Tables

Figures

◀

▶

◀

▶

Back

Close

Full Screen / Esc

Printer-friendly Version

Interactive Discussion

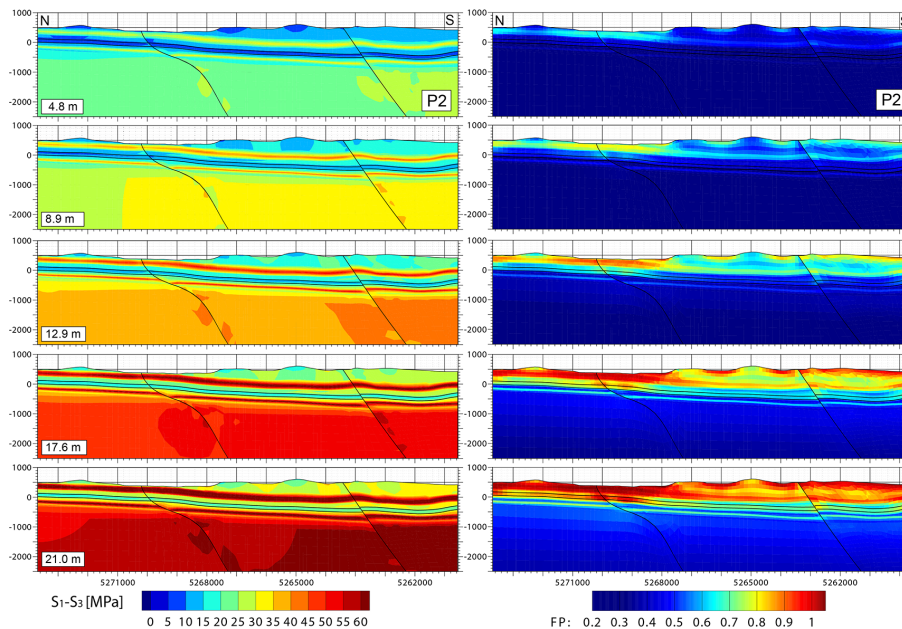


Figure 15. Additional south–north displacement of up to 21 m (total 30 m) and additional east and west displacement of up to 1.1 m each (total 3 m) of model BM in distinct steps displayed on north–south cross sections through the Weiach well. Thin black lines indicate top and bottom of the Opalinus Clay. Left column shows the gradual increase of the differential stress; right column shows the increase of the Fracture Potential (FP) which is the ratio of the actual differential stress to the yield stress using the plastic properties in each formation as stated in Table 1. FP values ≥ 1 indicate plastic failure of the formation.